JTTEE5 24:769–777
DOI: 10.1007/s11666-015-0237-z
1059-9630/$19.00 © ASM International

High-Temperature Oxidation and Hot Corrosion Studies on NiCrAlY Coatings Deposited by Flame-Spray Technique

Nidhi Rana, Manas Mohan Mahapatra, R. Jayaganthan, and Satya Prakash

(Submitted December 26, 2013; in revised form December 30, 2014)

The NiCrAlY coatings deposited by flame-spray technique on the superalloy substrate were oxidized in the presence of air and $Na_2SO_4 + V_2O_5$ salt at 900 °C for 100 cycles. The kinetics of oxidation showed that the coatings deposited by flame-spray technique possess better oxidation resistance compared with coatings deposited by high-velocity oxy fuel (HVOF)-sprayed technique. The oxidized coatings were further characterized by XRD, FESEM/EDS, and x-ray mapping techniques. The mechanisms of the oxidation and hot corrosion were substantiated by analyzing the results obtained from the various characterization techniques.

Keywords hot corrosion, molten salt, oxidation, SEM, Superalloy, XRD

1. Introduction

Oxidation and hot corrosion are the major degradation modes observed in power generation plants and turbine engines. Different types of coatings have been developed to protect the components from these degrading phenomena. Thermal-spray techniques such as flame spray, high-velocity oxy fuel (HVOF), plasma spray, D-gun, etc., are widely used for depositing the oxidation and corrosion-resistant coatings for high-temperature applications (Ref 1–5). Among them flame-spray or low-velocity oxy fuel (LVOF) process is an old conventional technique, which produces coatings with higher oxide contents and porosity compared with other advanced thermal-spray techniques. However, unlike other thermal-spray techniques, flame-spray technique is a cheap, simple, and low-energy thermal-spray process for spraying the coatings. Due to these reasons, flame-spray process is still used for deposition of the coatings on substrate to protect it against corrosion, erosion, and wear (Ref 6–12).

The oxidation and hot corrosion behaviors of the NiCrAlY coatings developed by various thermal-spray techniques have been studied extensively in the literature (Ref 13–19). In the case of high-temperature oxidation in the presence of air, the formation of slow-growing Al_2O_3 in the scale is found to provide the desired protection against high-temperature oxidation. However, formations of other oxides in the scale along with the stable alumina have also been reported (Ref 2). Some researchers have detected the θ alumina in early stages of the oxidation, the formation of which depends on temperature and time of the oxidation (Ref 13, 14). The amount of Al in the MCrAlY coating is also crucial for the formation of a pure α-Al_2O_3 scale as a protective layer on the surface to suppress the oxidation (Ref 15, 16). It was further investigated by Li et al. (Ref 17) that the chemical composition and the surface roughness also play important roles in the oxide formation. It has been reported that the Ni/Cr oxides along with Al_2O_3 were formed on the as-deposited cold-sprayed NiCrAlY coatings after high-temperature exposure, whereas in case of shot peened cold-sprayed NiCrAlY coatings, only Al_2O_3 was formed on the oxidized surfaces after exposure.

The hot corrosion resistance of the Ni-based coatings has been reviewed by Sidhu et al. (Ref 18). They concluded that the Ni-based coatings such as NiCr, Ni_3Al, NiCrBSi, and NiCrAlY exhibit good corrosion resistance due to the formation of oxides and spinels of Ni, Cr, and Al. The fireside corrosion behaviors of alloys 625, NiCr, FeCrAl, and NiCrAlY coatings deposited by HVOF- and the plasma-spray techniques at 650 °C were assessed by using a deposit containing Na_2SO_4, K_2SO_4, and Fe_2O_3 (Ref 19). It was concluded in their study that the plasma-sprayed coatings were more resistant to hot corrosion in a given environment compared with HVOF-sprayed coatings due to lesser porosity compared with HVOF-sprayed coatings.

The literature on oxidation and hot corrosion of the flame-sprayed coatings is limited. Hidalgo et al. (Ref 6) have compared the hot erosion behaviors of flame-sprayed and plasma-sprayed coatings. Before erosion test, they oxidized the coatings at 800 °C for 50 h. Weight gain of the flame-sprayed coatings during oxidation was similar to

Nidhi Rana, R. Jayaganthan, and **Satya Prakash**, Department of Metallurgical and Materials Engineering, Indian Institute of Technology Roorkee, Roorkee 247667, India; and **Manas Mohan Mahapatra**, Department of Mechanical and Industrial Engineering, Indian Institute of Technology Roorkee, Roorkee 247667, India. Contact e-mail: nidhiranathakur@gmail.com.

the weight gain of the plasma-sprayed coatings. However, adhesion of flame-sprayed coating was reported to be lower after oxidation, and the erosion increased due to the formation of cracks in the oxidized areas. Chaliampalias et al. (Ref 12) compared the oxidation behavior of the flame-sprayed and pack-cementation NiCrBSi coatings deposited on steel substrate. They observed that the performance of the flame-sprayed coatings was inferior to the pack-cemented coatings due to the formation of the FeO layer at the coating/alloy interface. The corrosion resistance of the coatings developed by different thermal-spray techniques (HVOF, flame spray, and arc spray) at 650 °C was studied by Rizzo et al. (Ref 20). They observed no significant changes in the corrosion behaviors of the coatings deposited by these techniques.

Flame spray is a cost effective and an easy-to-operate process compared with other thermal-spray techniques. Flame-pray technique has been studied mostly for depositing erosion-, and wear-resistant coatings. As per our knowledge, there are very few studies available which have studied the high-temperature oxidation behavior of flame-sprayed coatings (Ref 6, 12, 20). Owing to the above facts, in the present study, NiCrAlY coatings were deposited on superalloy substrate by using flame-spray technique. The oxidation and hot corrosion behavior of NiCrAlY coatings were investigated at 900 °C for 100 cycles. The suitability of the flame-spray method for the development of protective coatings against high-temperature oxidation and hot corrosion was assessed.

2. Experimental

2.1 Coating Deposition

Superni 76 procured from M/S MIDHANI, Hyderabad, India was used as substrate alloy for depositing the NiCrAlY coatings by using flame-spray process. The alloy was obtained in the form of the rolled sheets from which the samples of desired dimensions (20 mm × 15 mm × 3 mm) were cut. The nominal composition of the superni 76 as supplied by manufacturer has been shown in Table 1. All the six phases of the samples were polished by using SiC abrasive papers up to 1000 grit to achieve uniform and flat surface. After polishing, grit blasting of the samples was carried out by using irregular shaped alumina particles blown at an angle of 90° ± 10° with respect to the sample position. The roughness of the samples was measured by surface profilometer (SJ-400, Mututoyo, Japan). The average roughness of the samples was found to be 5.9 Ra. The commercially available NiCrAlY (Praxair Inc., US) powder having average particle size of ~40 μm with nominal composition (Cr-21 wt.%, Al-10 wt.%, Y-1 wt.%, Ni-bal) was used as feedstock powder to deposit the coatings on all six phases of the samples. The powder was preheated at 150 °C in an electric oven to remove moisture if present, and this heated powder was sprayed by using flame-spray (5PM-II Thermal Spray Gun, Jodhpur, India) technique. The various parameters used during deposition are given in Table 2.

Table 1 Composition of substrate superalloy (Superni76) as supplied by manufacturer

Element	Ni	Cr	Fe	Mo	W	Ti	Al	Co	Mn	C	Si
Wt%	Bal	21.49	19.69	9.05	0.6	…	…	1.6	0.29	0.86	0.39

2.2 Cyclic Oxidation and Hot Corrosion Test

Cyclic oxidation and hot corrosion tests were carried out up to 100 cycles (each cycle consists of 1 hour heating followed by 20 minutes cooling in air) at temperature 900 °C. Weight gain per unit area versus number of cycles plots were obtained for both cyclic oxidation in the presence of air and salt.

2.2.1 Cyclic Oxidation Test in the Presence of Air. Before oxidation test, the alumina boats were heated at 1100 °C to ascertain constant weight. The boats carrying samples were loaded in the SiC tubular furnace maintained at 900 °C. The samples were kept in the furnace for 1 h and then cooled in air for 20 min. This was continued for 100 cycles of the oxidation and weight was measured after each cycle by using weighing balance with sensitivity 10^{-4} g.

2.2.2 Cyclic Oxidation Test in the Presence of Salt (Hot Corrosion). The salt ($Na_2SO_4 + 60\%\ V_2O_5$) was mixed in the distilled water to get slurry of the same. This slurry (3-5 mg cm^{-2}) was applied uniformly on all six faces of the heated (150 °C) samples by using camel paint brush. The samples were weighed and were oxidized in SiC tubular furnace at 900 °C up to 100 cycles. The spalled scale was also included in the weight measurement. Weight gain per unit area versus number of cycles plots were obtained for both cyclic oxidation in the presence of air and salt.

2.3 Characterization Techniques

The phase identification of the as-sprayed coating and the oxidized samples were carried out by using x-ray Diffraction (Bruker AXS D-8Advance Diffractometer with Cu Kα radiation). The morphological and compositional analysis of the various samples was performed by using FESEM/EDS (FEI Company, Quanta 200F). The cross sectional images were taken by cutting the samples by using low speed precision diamond saw (MS-10, Ducom, India) in transverse direction and polishing with standard metallographic techniques. The porosity of the coating was measured by using image analyzer software (Dewinter Material Plus), by processing the micrograph obtained from optical microscope (Olympus DME3), as

Table 2 Spray parameters during deposition of NiCrAlY coatings by LVOF process

Oxygen flow rate	35 L min^{-1}
Acetylene flow rate	30 L min^{-1}
Powder feed rate	8 g min^{-1}
Distance b/w torch and sample	15 cm
Deposition time	50 s

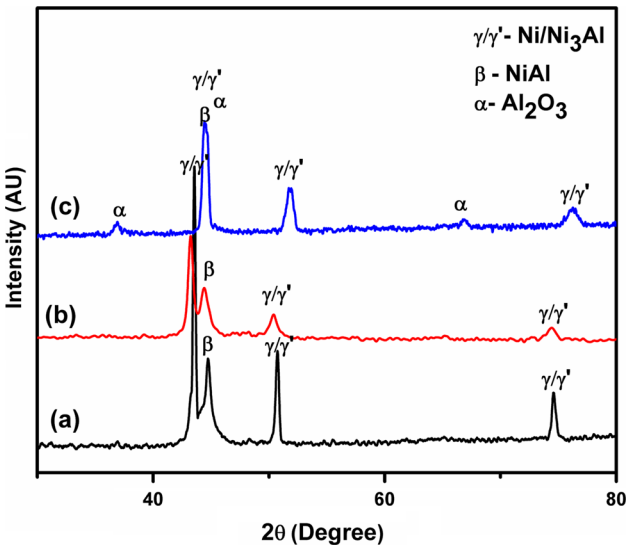

Fig. 1 XRD patterns of (a) NiCrAlY powder, (b) As-deposited HVOF-sprayed NiCrAlY coatings, and (c) As-deposited Flame-sprayed coating

per ASTM standard (E2109-01(2007)). The porosity was measured both on the surface and in the cross section of as-deposited coatings. The microhardness of the coating was measured in the cross section of the polished samples by using 402MVD (Wilson Instruments). A 100 g load was applied to the indenter for penetration of as-sprayed coatings. Each reported value of microhardness and porosity is the average of the five independent measurements taken at similar positions.

3. Results

3.1 As–Sprayed Flame–Sprayed Coatings

3.1.1 Phase Analysis. The XRD patterns of NiCrAlY powder and as-sprayed LVOF coating are shown in Fig. 1. The Al_2O_3 peaks correspond to the oxidation of the Al during the deposition process. The inherent low velocities used during the process causes oxidation of the powder. Shifting of the peaks corresponding to the γ/γ' phase was observed, which is attributed to the partial melting and rapid solidification of the powder during thermal-spray process. However, the peaks corresponding to γ/γ' phase has been shifted by a larger amount compared with the observed shifts in other thermal-spray processes. In author's previous studies, the HVOF-sprayed NiCrAlY coatings were obtained on the same substrate (superni76) by using same feedstock powder as used in the present study (Ref 21). For comparison purpose the XRD pattern of the HVOF-sprayed coatings has been also included in Fig. 1. It has been found that the peak shifts corresponding to the γ/γ' phase in case of HVOF coating is ~(0.21°, 0.23°, 0.21°), whereas the shifts in case of flame-sprayed coating is ~(1.1°, 1.3°, 1.5°).

The larger amount of peak shift is attributed to the larger amount of oxides (Al_2O_3) formation during deposition. In the author's previous study on HVOF-sprayed NiCrAlY coatings (by using same feedstock powder) the amount of oxides formed is negligible so does not affect the coating composition. However in flame-sprayed coatings Al gets oxidized extensively during deposition. Hence the larger peak shift is attributed to the formation of new phase (Al_2O_3) in the coating. Moreover the larger amount of shift in present case can also be attributed to generation of secondary cooling stresses due to large thermal mismatch between coating (partially oxidized, Al_2O_3 phases) and the substrate (metallic alloy) (Ref 22).

3.1.2 Surface and Cross Section Morphology. The surface morphology of the as spayed coatings shows the presence of splats with un-melted and semi-melted particles of the powder. The BSEI of the polished surface reveals the oxidation of the coating between the coating splats (Fig. 2b). The approximate thickness of the as-deposited flame-sprayed coatings is ~180 μm as estimated from the BSEI of the cross section (Fig. 3a). The cross section image (Fig. 3a) of the coatings shows the oxidized area between the splats. This type of the oxidized areas around the splats is the peculiar characteristics of the flame-sprayed NiCrAlY coatings and has not been reported in literature as per the authors' best knowledge. The porosities were calculated to be ~6% on the surface and ~5% along the cross section. The EDS and x-ray mapping results as shown in Fig. 3(b) confirm that the oxidized portion of the coatings is rich in Al and O with some amount of Cr. The EDS analysis and XRD results both are indicating the formation of alumina-rich regions around the splats. For the unoxidized regions of the as-sprayed coating, microhardness value was found to be 380 Hv, whereas the oxidized areas have a value of nearly 585 Hv. Similar observations have also been reported by Redjdala et al. (Ref 23).

3.2 Oxidation and Hot Corrosion Studies

3.2.1 Visual Observations. It has been observed that the coating color changed from dark gray to grayish black after five cycles of oxidation in air and then remain the same up to 100 cycles. In case of hot corrosion, the dark gray color has changed to dark greenish color after five cycles of exposure in the presence of molten salt. No cracks and spallation were observed up to 100 cycles of oxidation in air, whereas a little amount spallation was seen at the edges after 25 cycles of hot corrosion. This observation indicated that despite inherent lower velocities (~240 m s^{-1}) impacting the substrate; flame-spray technique can produce coatings with sufficient bond strength which can sustain stresses generated during cyclic oxidation.

3.2.2 Kinetics of Oxidation and Hot Corrosion. The weight change curves for the flame-sprayed and HVOF-sprayed coatings in the presence of air and salt are shown in Fig. 4. The curves tend to follow parabolic rate law of oxidation. The least square fit method was used to calculate the parabolic rate constants (K_p) for various curves as

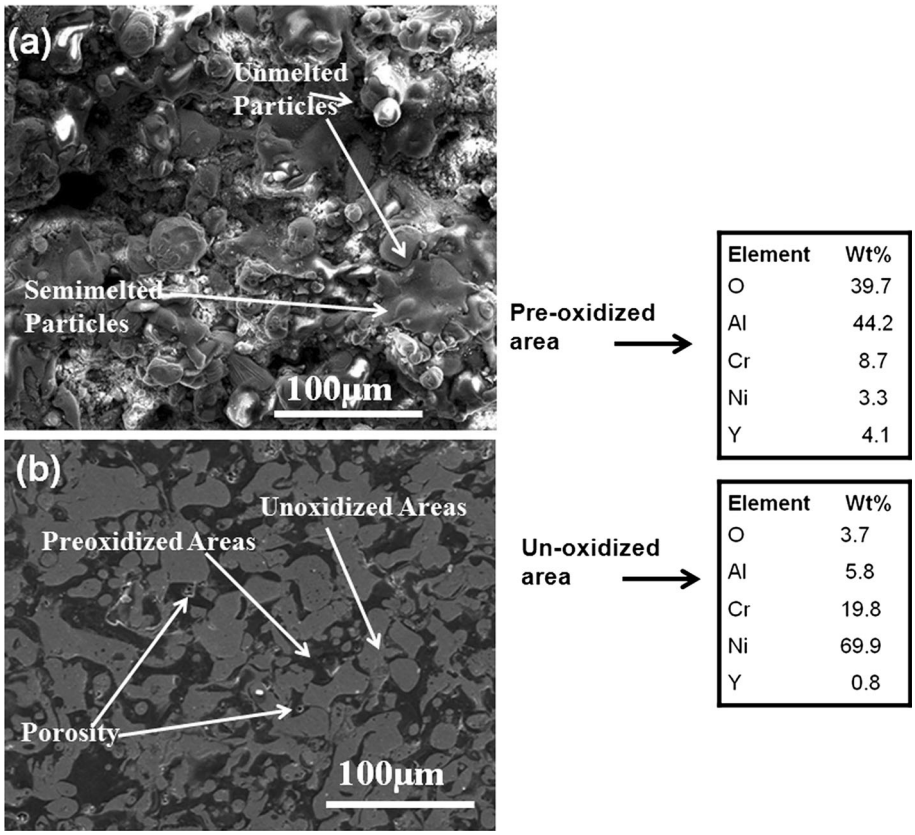

Fig. 2 Surface morphologies of the as-deposited Flame-prayed coatings: (a) without polishing and (b) after polishing (BSEI). Tables are showing the EDS compositions of the preoxidized and unoxidized regions of the coatings

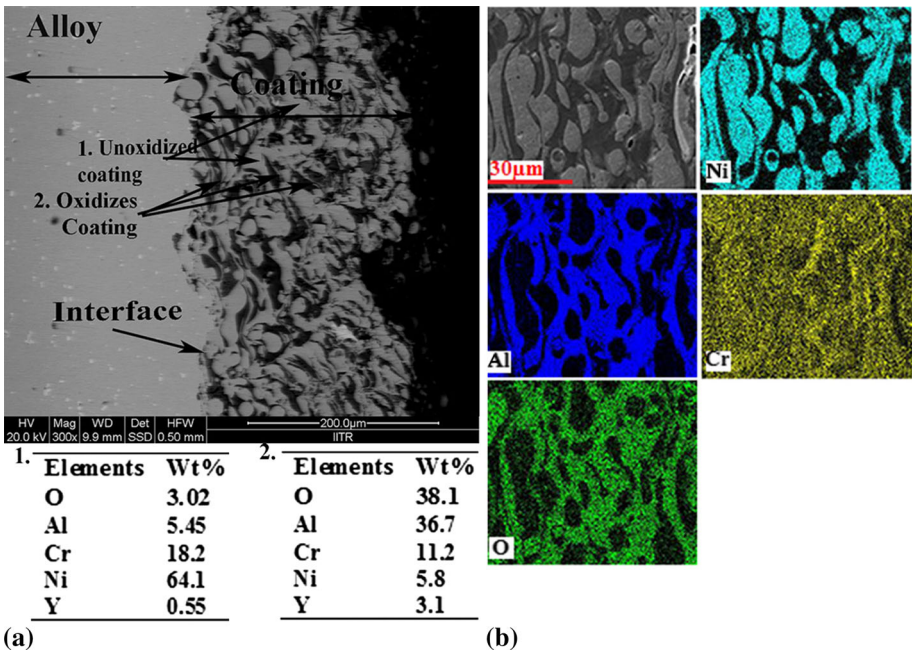

Fig. 3 (a) BSEI of the cross sections showing EDS of the oxidized and unoxidized areas, and (b) Elemental mapping in the cross section

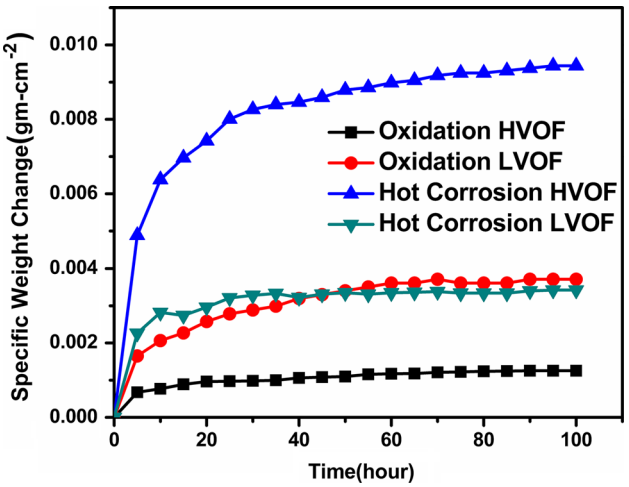

Fig. 4 Weight change curve for NiCrAlY coatings oxidized at 900 °C for 100 cycles

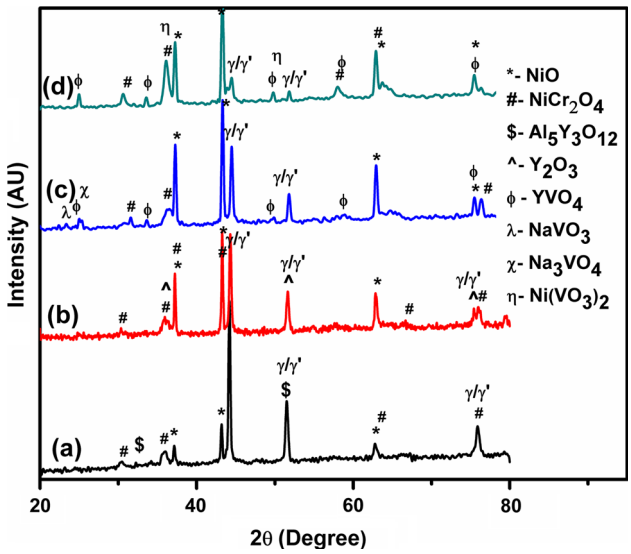

Fig. 5 XRD patterns of the flame-sprayed coatings after (a) 10 cycles of oxidation, (b) 100 cycles of oxidation, (c) 5 cycles of hot corrosion, and (d) 100 cycles of hot corrosion

Table 3 Parabolic rate constant of the oxidation and hot corrosion processes

Oxidation (HVOF sprayed)	3.1×10^{-12} g^2 cm^{-4} s^{-1}
Oxidation (LVOF sprayed)	2.8×10^{-11} g^2 cm^{-4} s^{-1}
Hot corrosion (HVOF sprayed)	1.4×10^{-10} g^2 cm^{-4} s^{-1}
Hot Corrosion (LVOF sprayed)	1.4×10^{-11} g^2 cm^{-4} s^{-1}

shown in Table 3. It can be seen that the weight gain of the flame-sprayed coatings in the presence of air is higher compared with HVOF coatings. However, in case of hot corrosion, the weight gain for flame-sprayed coatings is less than the HVOF coatings. It can be inferred that for the flame-sprayed coatings, weight gains in air and in the presence of salt were nearly the same. However, in case of HVOF coatings, there is a large difference between the two (8 times).

The oxidation and hot corrosion mechanisms of the same NiCrAlY coatings deposited by HVOF process has been reported in our earlier studies (Ref 24, 25) The weight change behavior and K_p values of HVOF coatings have been cited in this paper for comparing it with the LVOF-sprayed coatings in the present study.

3.2.3 XRD Analysis of the Air-Oxidized and Molten-Salt-Corroded Samples. The XRD patterns of the oxidized coatings in air and in the presence of salt are shown in Fig. 5. After 10 cycles of air oxidation, the main peak corresponding to NiO has appeared with small peaks of the spinels ($NiCr_2O_4$) and $Al_5Y_5O_{12}$. With the increasing number of cycles, the $NiCr_2O_4$ peaks became sharper with the appearance of Y_2O_3 peaks. After five cycles of hot corrosion, the peaks corresponding to Na_3VO_4, $NaVO_3$, YVO_4, and NiO oxides were observed. With the increasing number of cycles, the peaks corresponding to Na salt disappeared, and new peaks of Ni $(VO_3)_2$ appeared, while the peaks corresponding to NiO and spinels became prominent.

3.2.4 Surface Morphology and Composition. The surface morphologies of the oxidized samples in air and in the presence of salt are shown in Fig. 6. In case of air oxidation, the oxide crystals with distinct morphology have grown in the unoxidized portion of the coatings. These crystals are rich in Ni with little amounts of Cr and Al. The other region which is already oxidized during deposition shows no significant variation. After 100 cycles, the volume fraction of the oxide crystals increases with the oxidation of the unoxidized areas due to the formation of the mixed oxides, which are rich in Cr and Ni.

In case of hot corrosion, it has been observed that initially the surface is covered with Na- and V-rich salt along with the formation of some NiO. The rod-like structure rich in Y and V is also seen. Such types of rods have already been identified by others (Ref 26, 27). The Cr- and Al-rich oxides were also formed along with Ni-rich oxides. The compositions of the all the samples oxidized for different numbers of cycles are shown in Table 4.

3.2.5 Cross-Sectional Analysis. The cross-sectional images of the oxidized samples are shown in Fig. 7. The thickness of the oxide scale is only 6-7 μm after 100 cycles of air oxidation. It is clearly visible in the Fig. 7(a) that there are very few regions inside the coatings, which are oxidized during the cyclic oxidation experiment. The remaining part of the coatings showed the same phases as observed in the as-sprayed coating. In case of hot corrosion in the vanadate environment, the scale formed is thicker than that in air oxidation. The V has also penetrated into the coating at some places as shown in Fig. 7(b). The x-ray maps of the corroded samples are also shown in Fig. 8. It is evident from the Fig. 8(a) that the outer oxide layer is composed of Ni, Al, and Cr, while the rest of the coating is showing the same Al-rich pre-oxidized and Ni-rich unoxidized regions. Y has segregated at some places inside the coating. Figure 8(b) shows the

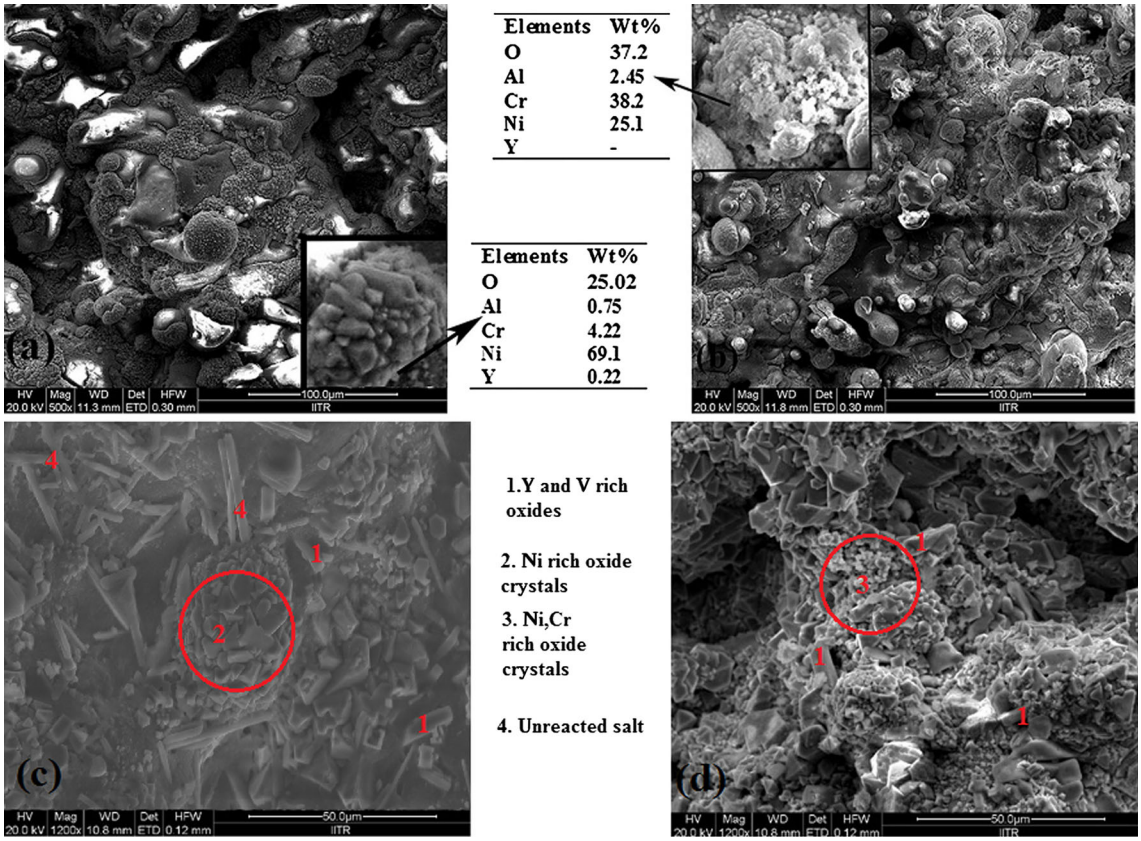

Fig. 6 Surface morphologies and EDS analyses of the flame-sprayed NiCrAlY coatings: (a) oxidized in air for 10 cycles, (b) oxidized in air for 100 cycles, (c) oxidized in the presence of salt for 5 cycles, and (d) oxidized in the presence of salt for 100 cycles

Table 4 Surface composition of the major coating elements of LVOF-sprayed NiCrAlY coatings (wt.%)

Element	As-sprayed coating	After oxidation 10 cycles	After oxidation 100 cycles	After hot corrosion 5 cycles	After hot corrosion 100 cycles
Al	23	14	11	3	2
Cr	14	17	24	8	13
Ni	28	31	26	38	40
Y	2	1.5	1.25	4.5	7.5
O	32	34	36	30	32
Na	…	…	…	12	1
V	…	…	…	3	4

penetration of the vanadium inside the coating at a few regions. It can also be observed that V and Y are present together at a few places. The outer scale again consists of Ni, Al, and Cr.

4. Discussion

The as-sprayed coatings exhibit a typical morphology composed of the oxidized and unoxidized areas. The EDS and XRD results show that the oxidized areas mainly consist of Al with some Cr. The XRD peaks reveal the presence of Al_2O_3 phase only. However, the x-ray maps clearly indicate the co-existence of the Al, Cr, and O. Hence, it can be inferred that the formation of $(Al, Cr)_2O_3$ solid solution occurs in which the Cr atoms substitutes some of the Al atoms in Al_2O_3 structure. Such type of formation of the solid solution of $(Al, Cr)_2O_3$ has been also observed in previous studies (Ref 28, 29). The extensive oxidation of Al can be explained on the basis of its high reactivity toward oxygen. Moreover, the composition of NiCrAlY powder is such that it promotes the selective oxidation of Al compared with Cr or Ni.

The weight-gain curve indicates that the coatings exhibit steady weight changes after an initial weight gain. It means that the oxygen uptake of the coatings become negligible after a certain number of cycles of oxidation, which shows that these coatings are protective up to 100

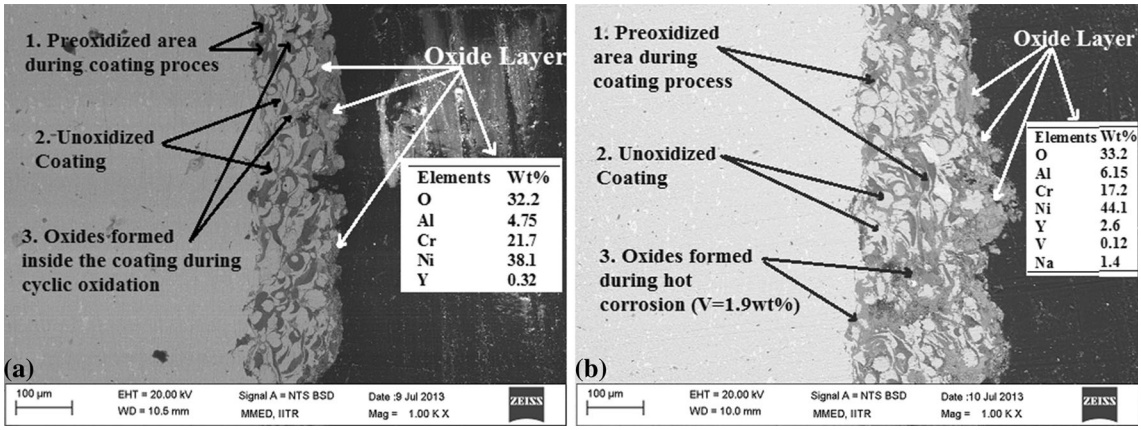

Fig. 7 BSEI of the cross sections of flame-prayed NiCrAlY coatings after 100 cycles of (a) oxidation in air and (b) oxidation in the presence of $Na_2SO_4 + V_2O_5$

cycles of oxidation and hot corrosion. The mechanisms of oxidation and hot corrosion of the LVOF coatings are explained as follows:

4.1 Oxidation of Preoxidized Areas

The preoxidized areas containing Al_2O_3 remains unaffected on exposure to oxidizing environment. As far as oxidation is concerned, it is a well-established fact that Al_2O_3 provides excellent protection against oxidation. Another reason for the better resistance of the Al_2O_3 formed is the presence of Y in this pre-oxidized areas, which contributes to the improved oxidation resistance (Ref 30). The appearances of the Y_2O_3 and $Al_5Y_3O_{12}$ have also been reported in the literature, wherein it has been suggested that these oxides contribute to reduce oxidation rate by binding the vacancies through which O can migrate (Ref 31). Hence, the preoxidized area provides the best protection against high-temperature oxidation.

Hot corrosion of the Al_2O_3 ceramics has been explained by formation of a liquid Na_2O-V_2O_5-(Al_2O_3) at a low temperature along the grain boundaries (Ref 29, 32). However, Hirata et al. (Ref 29) have observed that the hot corrosion resistance of Al_2O_3 increases when Cr atoms substitutes Al atoms in Al_2O_3 structure. The corrosion rate of the Cr_2O_3-Al_2O_3 ceramic is lower than that of Al_2O_3 ceramic due to the decrease in the dissolution rate of grains into the liquid phase compared with Al_2O_3 ceramics. The presence of YVO_4 has been observed in the coatings containing Y_2O_3 addition or the top coat of the yttria-stabilized zirconia YSZ (Ref 26, 33, 34). In the present case, the formation of the YVO_4 in early stages of corrosion is the indication that the Y is oxidizing rapidly to form Y_2O_3 and subsequently Y_2O_3 is reacting to form YVO_4. The reaction through which the YVO_4 forms was given by (Ref 34).

$$V_2O_5 + Na_2SO_4 \rightarrow 2(NaVO_3) + SO_3 \quad \text{(Eq 1)}$$

$$Y_2O_3 + 2(NaVO_3) \rightarrow 2YVO_4 + Na_2O \quad \text{(Eq 2)}$$

The presence of YVO_4 rods results in the spallation of the oxide scale due to the stress concentarions at the edges of the oxide rods. However, in the present case, the amount of the YVO_4 oxide is not sufficient to cause cracking and spallation of the oxide scale. The x-ray maps clearly indicate the formation of YVO_4 in a few regions only.

4.2 Oxidation of Unoxidized Areas

The unoxidized area of the as-sprayed coatings is rich in Ni and Cr with a little amount of Al. Hence, the relative concentration of the Al is not sufficient to form continuous Al_2O_3 layer during oxidation, due to which NiO and spinels have grown on the unoxidized portions of the coating. The effects of relative concentrations of the Ni, Cr, and Al on the oxide formation have been explained by Petit et al. (Ref 35). With the increasing oxidation time, the concentration of the spinels increases, which leads to the decreased oxidation rate as also evident from the weight-change curve. It has been reported that the spinel phase usually has lower diffusion coefficients of the cations and anions than those in their parent oxides (Ref 36).

In case of hot corrosion, the Ni reacts with the $NaVO_3$ and forms Ni vanadates. It has been reported earlier that the Ni $(VO_3)_2$ is a refractory oxide and acts as diffusion barrier for the oxidizing species (Ref 37). On the other hand, the spinels have lower solubility in the molten salt compared with NiO (Ref 38). Hence, the lower weight gain and minor spallation observed in case of hot corrosion can be explained on the basis of the improved hot corrosion performance of the (Al, $Cr)_2O_3$ system and the lower solubility of the NiC_2O_4 into the salt.

It may be mentioned that there is a large difference between the weight changes of HVOF and flame-sprayed coatings during hot corrosion. It can be explained on the basis of the better hot corrosion resistance of the Al_2O_3 compared with Cr_2O_3 (Ref 39). In our previous study (Ref 26) on hot corrosion of the HVOF-sprayed coatings, it has been found that the Cr gets depleted from the coating due to continuous dissolution of Cr_2O_3 in the $Na_2SO_4 + V_2O_5$

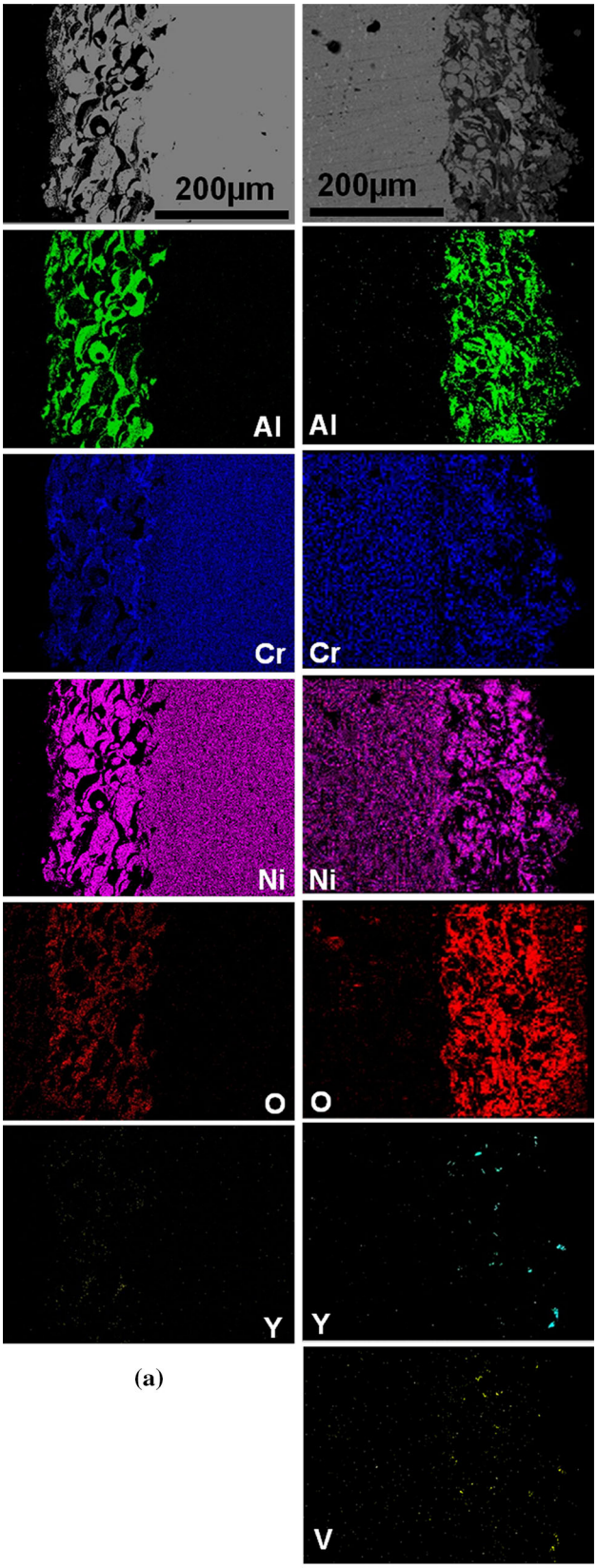

◀**Fig. 8** X-ray maps of the cross sections of the coatings after 100 cycles of (a) oxidation in air and (b) oxidation in the presence of $Na_2SO_4 + V_2O_5$

salt. The spallation as observed in case of HVOF-sprayed coatings is the consequence of fluxing of Cr_2O_3 in the salt, and consequently, the weight gain became faster. However, in the present case, the Al gets oxidized during deposition and formed the $(Al, Cr)_2 O_3$ in the preoxidized areas, and hence the dissolution of the scale and weight gain were slower.

5. Conclusions

The NiCrAlY coatings were successfully deposited on superalloy by using flame sprayed process in the present study. This coating provides optimal protection against high-temperature oxidation in air and in the molten-salt ($Na_2SO_4 + 60\% V_2O_5$) environment. The peculiar morphology of as-sprayed coatings showed preoxidized regions composed of alumina and the unoxidized regions containing Ni and Cr. This morphology inherently provides protection against air oxidation and is also resisting aggressive molten salt at 900 °C. In case of the molten-salt environment, the oxides of Ni, Cr, and spinels have grown throughout the whole surface. However, in case of air oxidation, the preoxidized area remained unaffected even after 100 cycles of oxidation. The porosity of the coatings showed minimal effect on the air oxidation. In case of hot corrosion, the V penetrated into the pores but did not intensify the corrosive attack. The formations of the $NiCr_2O_4$ and $Ni (VO_3)_2$ in the scale provide further protection against hot corrosion. Flame spray is a low-energy process and may prove to be more economic in providing protection against high-temperature oxidation and the molten-salt corrosion along with protection against wear and erosion as observed in the present study.

References

1. L.Y. Ni, C. Liu, H. Huang, and C.G. Zhou, Thermal Cycling Behavior of Thermal Barrier Coatings with HVOF NiCrAlY Bond Coat, *J. Therm. Spray Technol.*, 2011, **20**(5), p 1133-1138
2. Philip Puetz, Xiao Huang, Q. Yang, and Z. Tang, Transient Oxide Formation on APS NiCrAlY After Oxidation Heat Treatment, *J. Therm. Spray Technol.*, 2011, **20**(3), p 621-629
3. M. Kaur, H. Singh, and S. Prakash, Surface Engineering Analysis of Detonation-Gun Sprayed Cr3 C2–NiCr Coating Under High-Temperature Oxidation and Oxidation–Erosion Environments, *Surf. Coat. Technol.*, 2011, **206**, p 530-541
4. Niraj Bala, Harpreet Singh, Satya Prakash, and J. Karthikeyan, Investigations on the Behavior of HVOF and Cold Sprayed Ni-20Cr Coating on T22 Boiler Steel in Actual Boiler Environment, *J. Therm. Spray Technol.*, 2012, **21**(1), p 144-158
5. S. Matthews and M. Schweizer, High-Temperature Oxidation and Smelt Deposit Corrosion of Ni-Cr-Ti Arc-Sprayed Coatings, *J. Therm. Spray Technol.*, 2010, **19**(1–2), p 932-946
6. V. Higuera Hidalgo, J. Belzunce Varela, A. CarrilesMenéndeza, and S. Poveda Martínez, High temperature erosion wear of flame and plasma-sprayed nickel–chromium coatings under simulated coal-fired boiler atmospheres, *Wear*, 2001, **247**, p 214-222

7. B. Uyulgan, E. Dokumaci, E. Celik, I. Kayatekin, N.F. Ak Azem, I. Ozdemir, and M. Toparli, Wear Behaviour of Thermal Flame Sprayed FeCr Coatings on Plain Carbon Steel Substrate, *J. Mater. Process. Technol.*, 2007, **190**, p 204-210
8. S. Sharma, High Temperature Erosive Wear Study of NiCrFeSiB Flame Sprayed Coating, *J. Inst. Eng. Ser. D*, 2012, **93**(1), p 7-12
9. K.A. Habib, J.J. Saura, C. Ferrer, M.S. Damra, E. Giménez, and L. Cabedo, Comparison of Flame Sprayed Al_2O_3/TiO_2 Coatings: Their Microstructure, Mechanical Properties and Tribology Behaviour, *Surf. Coat. Technol.*, 2006, **201**, p 1436-1443
10. R. Gonźalez, M. Cadenas, R. Ferńandez, J.L. Cortizo, and E. Rodŕiguez, Wear Behaviour of Flame Sprayed NiCrBSi Coating Remelted by Flame or by Laser, *Wear*, 2007, **262**, p 301-307
11. Q. Wang, Z. Chen, Z.X. Ding, and D. Chen, Abrasive Wear Behaviour of WC Reinforced Ni Based Composite Coatings Sprayed and Fused by Oxy-Acetylene Flame, *Surf. Rev. Lett.*, 2009, **1**(3), p 475-485
12. D. Chaliampalias, G. Vourlias, E. Pavlidou, S. Skolianos, K. Chrissafis, and G. Stergioudis, Comparative Examination of the Microstructure and High Temperature Oxidation Performance of NiCrBSi Flame Sprayed and Pack Cementation Coatings, *Appl. Surf. Sci.*, 2009, **255**, p 3605-3612
13. M.H. Li, Z.Y. Zhang, X.F. Sun, J.G. Li, F.S. Yin, W.Y. Hu, H.R. Guan, and Z.Q. Hu, Oxidation Behavior of Sputter-Deposited NiCrAlY Coating, *Surf. Coat. Technol.*, 2003, **165**, p 241-247
14. D. Toma, W. Brandl, and U. Koster, The Characteristics of Alumina Scales Formed on HVOF-Sprayed MCrAlY Coatings, *Oxid. Met.*, 2000, **53**, p 125-137
15. N. Czech, F. Schmitz, and W. Stamm, Microstructural Analysis of the Role of Rhenium in Advanced MCrAlY Coatings, *Surf. Coat. Technol.*, 1995, **76--77**, p 28-33
16. J.W. Hutchinson and A.G. Evans, On the Delamination of Thermal Barrier Coatings in a Thermal Gradient, *Surf. Coat. Technol.*, 2002, **149**, p 179-184
17. Yong Li, Chang-Jiu Li, Qiang Zhang, Lu-Kuo Xing, and Guan-Jun Yang, Effect of Chemical Compositions and Surface Morphologies of MCrAlY Coating on Its Isothermal Oxidation Behavior, *J. Therm. Spray Technol.*, 2011, **20**(1–2), p 121-131
18. T.S. Sidhu, S. Prakash, and R.D. Agrwal, Hot Corrosion Performance of Nickel Based Coatings, *Curr. Sci.*, 2006, **90**, p 41-47
19. T. Hussain, T. Dudziak, N.J. Simms, and J.R. Nicholls, Fireside Corrosion Behavior of HVOF and Plasma-Sprayed Coatings in Advanced Coal/Biomass Co-Fired Power Plants, *J. Therm. Spray Technol.*, 2013, **22**(5), p 797-807
20. F. Rizzo, M. Monteiro, M.F. Lopes, I. Caminha, C. Zeng, and M. Piza Paes, Evaluation of the Corrosion Resistance of Thermal-Spray Coatings Under Oxidant Atmosphere in a Fluid Catalytic-Cracking Unit, *Oxid. Met.*, 2002, **57**, p 323-338
21. N. Rana, R. Jayaganthan, and S. Prakash, Microstructural Features and Oxidation Behaviour of NiCrAlY Coatings Obtained by HVOF Process, *Adv. Mater. Res.*, 2012, **585**, p 507-511
22. J. Matejicek and S. Sampath, Intrinsic Residual Stresses in Single Splats Produced by Thermal Spray Processes, *Acta Mater.*, 2001, **49**, p 1993-1999
23. O. Redjdal, B. Zaid, M.S. Tabti, K. Henda, and P.C. Lacaze, Characterization of Thermal Flame Sprayed Coatings Prepared from FeCr Mechanically Milled Powder, *J. Mater. Process. Technol.*, 2013, **213**, p 779-790
24. N. Rana, R. Jayaganthan, and S. Prakash, Stepwise Oxidation Mechanism of HVOF Sprayed NiCrAlY Coatings in Air, *T Indian I, Metals*, 2014, **67**, p 393-400
25. N. Rana, R. Jayaganthan, and S. Prakash, Stepwise Depletion of Coating Elements as a Result of Hot Corrosion of NiCrAlY Coating, *J. Mater. Eng. Perform.*, 2014, **23**, p 643-650
26. G. Sreedhar, M. Alam, and V.S. Raja, Hot Corrosion Behaviour of Plasma Sprayed YSZ/Al_2O_3 Dispersed NiCrAlY Coatings on Inconel-718 Superalloy, *Surf. Coat. Technol.*, 2009, **204**, p 291-299
27. X. Chena, Y. Zhao, L. Gua, B. Zou, Y. Wang, and X. Cao, Hot Corrosion Behaviour of Plasma Sprayed YSZ/LaMgAl11O19 Composite Coatings in Molten Sulfate–Vanadate Salt, *Corros. Sci.*, 2011, **53**, p 2335-2343
28. J. Ma, S.M. Jiang, J. Gong, and C. Sun, Behaviour and Mechanisms of Alkali-Sulphate-Induced Hot Corrosion on Composite Coatings at 900 °C, *Corros. Sci.*, 2012, **58**, p 251-259
29. T. Hirata, K. Akiyama, and H. Yamamoto, Corrosion Resistance of Cr_2O_3-Al_2O_3 Ceramics by Molten Sodium Sulphate–Vanadium Pentoxide, *J. Mater. Sci.*, 2001, **36**, p 5927-5934
30. T.A. Ramanarayana, Metallic Y Addition to High Temperature Alloys: Influence on Al_2O_3 Scale Properties, *Oxid. Met.*, 1984, **22**, p 83-100
31. E.W.A. Young and J.H.W. Wit, An ^{18}O Tracer Study on the Growth Mechanism of Alumina Scales on NiAl and NiAlY Alloys, *Oxid. Met.*, 1986, **26**, p 351-361
32. L.A. Klinkova and E.A. Ukshe, *Zh. Neorg. Khim.*, 1975, **20**(2), p 481
33. S. Mohsen, A. Abbas, and K. Akira, Bond Coat Oxidation and Hot Corrosion Behaviour of Plasma Sprayed YSZ Coating on Ni Based Superalloy, *Trans. JWRI.*, 2007, **36**, p 41-45
34. C. Batista, A. Portinha, R.M. Ribeiro, V. Teixeira, and C.R. Oliveira, Evaluation of Laser-Glazed Plasma-Sprayed Thermal Barrier Coatings Under High Temperature Exposure to Molten Salts, *Surf. Coat. Technol.*, 2006, **200**, p 6783-6791
35. C.S. Giggins and F.S. Pettit, Oxidation of NiCrAl alloys between 1000-1200 °C, *J. Electrochem. Soc. Solid State Sci.*, 1971, **118**, p 1782-1790
36. U.K. Chatterjee, S.K. Bose, and S.K. Roy, *Environmental Degradation of Metals*, Marcel Dekker, New York, 2001
37. Gitanjaly, *Role of Inhibitors on Hot Corrosion of Superalloys in Na_2SO_4-V_2O_5Environment*. Ph.D. Thesis, Met. Mater. Eng. Dept., Indian Institute of Technology Roorkee, Roorkee, India, 2003
38. W.H. Lee and R.Y. Lin, Hot Corrosion Mechanism of Intermetallic Compound Ni_3Al, *Mater. Chem. Phys.*, 2003, **77**(1), p 86-96
39. J.A. Goebel, F.S. Pettit, and G.W. Goward, Mechanisms for the Hot Corrosion of Nickel-Base Alloys, *Metall. Mater. Trans. A*, 1973, **4**(1), p 261-278